Hindawi
Journal of Chemistry
Volume 2018, Article ID 8418605, 9 pages
https://doi.org/10.1155/2018/8418605

*Research Article*

# Synthesis of Al-MCM-41@Ag/$TiO_2$ Nanocomposite and Its Photocatalytic Activity for Degradation of Dibenzothiophene

**Xuan Nui Pham ,[1] Tuan Dat Pham,[1] Ba Manh Nguyen,[1,2] Hoa Thi Tran,[2,3] and Dinh Trong Pham[4]**

[1]*Department of Chemical Engineering, Hanoi University of Mining and Geology, 18 Duc Thang, Bac Tu Liem, Hanoit, Vietnam*
[2]*Vietnam Academy of Science and Technology, 18 Hoang Quoc Viet, Hanoi, Vietnam*
[3]*Department of Chemical Engineering, Viet Tri University of Industry, 9 Tien Son Str., Viet Tri City, Vietnam*
[4]*Faculty of Chemistry, Hanoi University of Science, Vietnam National University, 19 Le Thanh Tong, Hoan Kiem, Hanoi, Vietnam*

Correspondence should be addressed to Xuan Nui Pham; phamxuannui@gmail.com

Received 11 June 2018; Accepted 16 October 2018; Published 5 December 2018

Academic Editor: Stefano Caporali



Mesoporous Al-MCM-41@Ag/$TiO_2$ nanocomposites were synthesized successfully by combining the sol-gel method and hydrothermal treatment, using titanium isopropoxide (TTIP), $AgNO_3$, and Vietnamese bentonite as precursors of Ti, Ag, and Si, respectively. The synthesized materials were well characterized by X-ray powder diffraction (XRD), scanning electron microscopy (SEM), transmission electron microscopy (TEM), $N_2$ adsorption-desorption isotherm measurements, energy dispersive X-ray spectroscopy (EDX), UV-visible diffuse reflectance spectroscopy (UV-Vis/DRS), and X-ray photoelectron spectroscopy (XPS). The photocatalytic activity was evaluated by the photodegradation of dibenzothiophene (DBT) under both UV and visible light irradiation. MCM-41@Ag/$TiO_2$ catalyst exhibited high catalytic activity for the oxidative desulfurization (ODS) of DBT reaching almost 100% conversions at 50°C after 2 h under UV and visible light irradiations. The significant enhanced degradation of DBT over Al-MCM-41@Ag/$TiO_2$ might be due to the synergy effects of high surface area of MCM-41, well-distributed $TiO_2$ anatase, and reduced electron-hole recombination rates due to the dispersion of Ag nanoparticles.

## 1. Introduction

Dibenzothiophene presenting in diesel is one of the main sulfur-containing organic pollutants in fuel oils and is difficult to be removed [1]. This organic pollutant is difficult to be reduced using the conventional hydrodesulfurization (HDS) due to its steric hindrance [2, 3]. Photocatalytic oxidation is one of the most promising pollution treatments to remove many organic pollutants in water [4] and air steam [5]. Due to more stringent environmental regulations, it is critical to develop effective photocatalysts for the removal of sulfur-containing organic compounds from fuel oils through photocatalytic oxidation processes. Titanium dioxide ($TiO_2$) has been well known and was the most widely studied semiconductor photocatalyst due to its low cost, nontoxicity, and high chemical stability [6]. However, the semiconductor $TiO_2$ has a wide band gap (3.0–3.2 eV) that strongly restricted its application because the material only absorbs a small fraction of the solar photons (the UV light occupies about 5% of the total solar energy). Besides, high recombination between electrons ($e^-$) and holes ($h^+$) results in reduced photocatalytic efficiency [7, 8].

The incorporation and doping of noble metal nanoparticles (e.g., Ag, Au, and Pt) into the crystal lattice of $TiO_2$ (metal-$TiO_2$) to absorb the abundant visible light due to their surface plasmon resonance (SPR) have been investigated to overcome this limitation in the $TiO_2$ photocatalyst material [9–12]. Silver has an advantage of having a lower cost compared with gold or platinum. However, the use of metal-$TiO_2$ powders in the treatment of aqueous organic pollutants has some drawbacks such as difficult recovery and poor adsorption capacity due to its low surface area and agglomeration in suspension [13]. Therefore, noble metal nanoparticles doping on titania with improved crystallinity, surface area, and surface properties to achieve higher adsorption capacity and photocatalytic activity [14] have been studied extensively such as metal-titania nanoparticles coated on the high surface area supports and thermally stable core materials [15, 16]. Nanoporous materials such as ordered mesoporous silica [17–19], activated carbon [20, 21], microporous zeolites [22, 23], and metal organic frameworks [24, 25] have been widely used as $TiO_2$ carriers due to their versatile structures and high porosity to achieve more active sites per unit area, consequently, a higher photocatalytic reaction rate. Mesoporous aluminosilicate Al-MCM-41 is one of the most widely used support materials due to its remarkable acidic properties, high thermal and mechanical stability, highly ordered hexagonal structure, and high surface area [26–30]. Recent studies have focused on the use of low-cost raw materials, particularly in their natural forms such as bentonite clay to synthesize high value products. The inorganic components consisting of silica and alumina were collected by annealing bentonite with sodium hydroxide at a temperature higher than 500°C to use for the synthesis of Al-MCM-41 [31, 32]. Herein, the Al-MCM-41 mesoporous material was prepared by a hydrothermal method using the Vietnamese bentonite as Si and Al precursors. Then, $Ag/TiO_2$ nanoparticles were deposited on the surface of the Al-MCM-41 material to improve the dispersion of $TiO_2$, and the synthesized Al-MCM-41@$Ag/TiO_2$ nanocomposites were used as a photocatalyst for the oxidative desulfurization of dibenzothiophene under both UV and visible light irradiation.

## 2. Experimental

*2.1. Chemicals.* Dibenzothiophene (DBT), triblock Pluronic F127 ($EO_{106}PO_{70}EO_{106}$, 99 wt%, $M$ = 12.600), titanium (IV) isopropoxide (TTIP, 97 wt%), *n*-octane (99 wt%), silver nitrate (99 wt%), cetyltrimethylammonium bromide (CTAB, 98 wt%), ethanol (99.5 wt%), acetic acid (99 wt%), hydrogen peroxide (30%wt), and NaOH (98%wt) were purchased from either Sigma-Aldrich or Merck. Bentonite was obtained from Di Linh, Vietnam, with a chemical composition of 52 $SiO_2$ : 15 $Al_2O_3$ : 11 $Fe_2O_3$ : 0.8 $TiO_2$ : 2 CaO : 3.5 MgO : 2 $Na_2O$ in weight percent and the loss on ignition (LOI) of 13.7%.

*2.2. Synthesis of Al-MCM-41 from Vietnamese Bentonite.* Firstly, Si and Al precursors were obtained following the protocol described by Ali-dahmane et al. [31]. The Vietnamese bentonite was mixed with sodium hydroxide (NaOH) in bentonite : NaOH weight ratio of 1 : 1.2 and heated at 550°C for 3h in air. The fused bentonite obtained was cooled, milled, mixed with distilled water with a weight ratio of 1 : 4, and then stirred at room temperature for 24 h. The supernatant was separated by centrifugation to obtain the Si and Al precursors.

In a typical Al-MCM-41 synthesis, 1.2 g CTAB was added to 20 mL distilled water. Then, 42 mL of the supernatant was added to the above solution and stirred at room temperature for 6 h at pH of about 9-10, which was adjusted by acetic acid. The crystallization step was carried out at 100°C in a stainless steel autoclave for 24 hours. The white precipitate was then filtered and washed three times with distilled water and ethanol and dried overnight at 100°C. Finally, the template CTAB was removed by calcining at 550°C for 6 h in air.

*2.3. Synthesis of Al-MCM-41@nAg/$TiO_2$ Nanocomposite.* Al-MCM-41@nAg/$TiO_2$ nanocomposite microspheres were synthesized by a sol-gel method. 0.1 g of the synthesized Al-MCM-41 was dispersed in 100 mL ethanol via sonication for 1 h. Then, 0.2 g F127 and 2 mL distilled water were added to the above solution. The mixture was stirred at 50°C for 30 minutes.

A $TiO_2$ precursor (solution A) was prepared by dissolving titanium(IV) isopropoxide (TTIP) in a mixed solvent of ethanol and nitric acid to form a final composition of 1 TTIP : $C_2H_5OH$ : 2 $H_2O$ : 0.2 $HNO_3$. Solution B was prepared by adding $n$% ($n$ = 5, 10, and 15) moles of $AgNO_3$ into 15 mL ethanol and stirred for 30 minutes. Then, solution A was mixed with solution B and stirred vigorously for 30 minutes. The $Ag/TiO_2$ precursor was added dropwise to the Al-MCM-41 suspension to obtain Al-MCM-41@nAg/$TiO_2$. The temperature was then increased to 80°C under refluxing conditions for 6 h. The solid was collected by centrifugation and washed thoroughly with ethanol and dried at 80°C. Finally, F127 was removed by calcining the obtained solid at 450°C in air for 5 h.

*2.4. Oxidative Photodesulfurization of Dibenzothiophene.* Dibenzothiophene was dissolved in *n*-octane to create a model fuel with known sulfur content in ppm. Next, 20 mL of DBT/*n*-octane solution was placed in a 500 ml three-neck round-bottom flask containing 0.05 g catalyst. The suspension was stirred for 30 minutes in the dark and then was illuminated with two 15 W UV lamps (UV light) or a 165 W tungsten lamp (visible light) at various temperatures (30°C, 50°C, and 70°C) under refluxing conditions for 5 h. 0.5 mL of $H_2O_2$ as an oxidative agent was added to the mixture at the reaction temperatures. After certain reaction time, small amounts of the products were taken out, centrifuged, and analyzed by high-performance liquid chromatography (HPLC). Then, peak areas were converted to their corresponding concentrations through the standard curves. The percentage of degradation of DBT ($\eta$) was calculated according to the initial, $C_0$ (ppm), and final, $C$ (ppm), concentrations of DBT in the solution following this equation: $\eta = 100 \times (C_0 - C)/C_0$.

*2.5. Characterization.* Powder X-ray diffraction (XRD) patterns were recorded on a D8-Advance Bruker with Cu-K$\alpha$ radiation ($\lambda$ = 0.15406 nm) as the X-ray source at a scan rate of 0.3°–0.6° $min^{-1}$. Transmission electron microscopy (TEM) images were taken by a TEM TECNAI G 2 20 with an accelerating voltage of 200 kV. Scanning electron microscopy (SEM) images were obtained on an S4800-Hitachi. Pore size distributions were calculated from $N_2$ isotherms using the

Barrett–Joyner–Halenda (BJH) model. Energy dispersive X-ray (EDX) spectra were measured on a JED-2300 instrument. The surface electronic states identified through X-ray photoelectron spectroscopy (XPS) were taken on an AXIS ULTRA DLD Shimadzu–Kratos spectrometer using monochromatic X-rays Al-K$\alpha$ radiation (1486.6 eV). UV-Vis diffuse reflection spectroscopy (UV-Vis/DRS) was performed on a Shimadzu UV2550 spectrophotometer with a $BaSO_4$-coated integrating sphere in the wavelength range of 200–800 nm.

## 3. Results and Discussion

*3.1. Characterizations of the Synthesized Materials.* Wide-angle XRD patterns of Al-MCM-41, Al-MCM-41@$TiO_2$, and Al-MCM-41@Ag/$TiO_2$ with different Ag concentrations are shown in Figure 1. The XRD pattern of Al-MCM-41 (Figure 1(e)) does not have diffraction peaks in the range of 15° to 30°, indicating a characteristic of amorphous silica walls of the pristine material. In contrast, Al-MCM-41@$TiO_2$ (Figure 1(d)) and Al-MCM-41@Ag/$TiO_2$ (Figures 1(a)–1(c)) contain diffraction peaks at $2\theta = 25.4°$; 37.9°; 48.4°; 54.0°; 55.2°; and 62.8° corresponding to (101), (004), (200), (105), (211), and (204) planes of a typical $TiO_2$ anatase phase, respectively [33]. Al-MCM-41@Ag/$TiO_2$ composites contain obvious diffraction peaks of $TiO_2$, but no typical peaks of Ag were observed. This might be due to the low concentration of Ag, or the typical diffraction peaks of Ag were covered by a (004) diffraction peak of the $TiO_2$ anatase. The presence of Ag in the Al-MCM-41@Ag/$TiO_2$ composites will be discussed later using EDX and XPS methods.

Figure 1 (inset) is the small angle XRD results of Al-MCM-41, Al-MCM-41@$TiO_2$, and Al-MCM-41@Ag/$TiO_2$. Diffraction peaks at $2\theta = 2.3°$; 3.9°; and 4.5° of the Al-MCM-41 sample were assigned, respectively, to (100), (110), and (200) planes associated with a p6mm hexagonal symmetry of a mesoporous material with highly uniform and ordered structure. However, the peak intensities at $2\theta = 2.3°$ were significantly reduced, and the other peaks at 3.9° and 4.5° were not clear (Figures 1(a)–1(d) (inset)). This could be due to the existence of $TiO_2$ and Ag/$TiO_2$ inside the channels of Al-MCM-41@$TiO_2$ and Al-MCM-41@Ag/$TiO_2$ materials.

SEM images of Al-MCM-41 and Al-MCM-41@0.1Ag/$TiO_2$ are shown in Figure 2. The SEM images of Al-MCM-41 revealed irregular spherical particles with a cross-linked network and a particle size of about 120 nm. The average particle size of Al-MCM-41@0.1Ag/$TiO_2$ (150 nm) was larger than that of Al-MCM-41 nanoparticles, which indicated a possible coverage of $TiO_2$ nanoparticles having a thickness of about 15 nm on the surface of the Al-MCM-41@0.1Ag/$TiO_2$ nanocomposite.

Figures 3(a) and 3(b) are the TEM images of Al-MCM-41@0.1Ag/$TiO_2$ catalyst. The TEM images showed that the nanocomposite possesses ordered mesoporous channels with a slight decrease in the orderly porous structure as compared to the parent Al-MCM-41 material, which is in agreement with the XRD result. The Ag/$TiO_2$ particles having the size of about 5–15 nm were well-dispersed on the surface and mesopore of the Al-MCM-41 support.

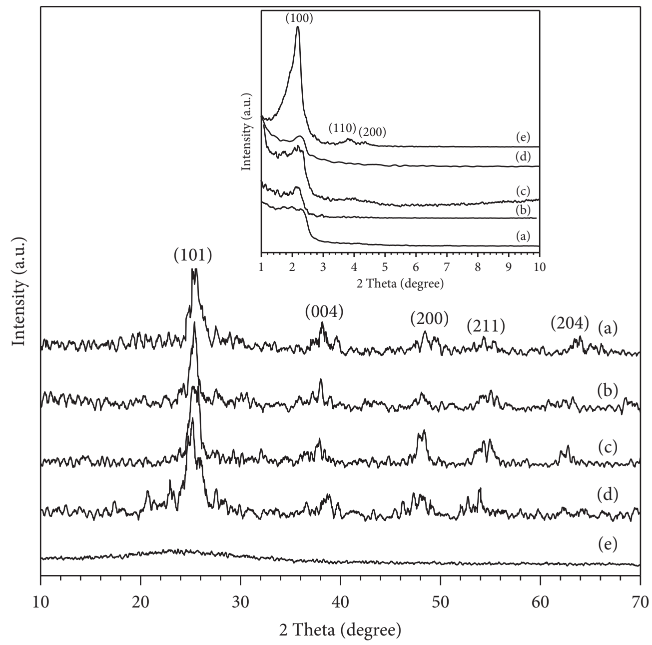


Figure 1: XRD patterns of (a) Al-MCM-41@0.15Ag/$TiO_2$, (b) Al-MCM-41@0.1Ag/$TiO_2$, (c) Al-MCM-41@0.05Ag/$TiO_2$, (d) Al-MCM-41@$TiO_2$, and (e) Al-MCM-41. Inset is the small angle X-ray diffraction patterns.

The UV-Vis diffuse reflectance spectra of Al-MCM-41, Al-MCM-41@$TiO_2$, and Al-MCM-41@nAg/$TiO_2$ composites in the range of 250–800 nm are shown in Figure 4. The strong UV absorption spectrum of Al-MCM-41@$TiO_2$ observed at strong absorption band at wavelengths from 250 to 380 nm, with the sharp absorption edge of about 330 nm, is attributed to the intrinsic band gap absorption of anatase $TiO_2$ [34]. Al-MCM-41@0.1Ag/$TiO_2$ and Al-MCM-41@0.15Ag/$TiO_2$ containing a high amount of Ag nanoparticles showed a light absorption band in the visible region with peaks at about 435 nm. This could be related to the localized surface plasmon resonance effect of silver nanoparticles [35], which varies with the Ag content of MCM-41@Ag/$TiO_2$ nanostructures. The band gaps of the composite samples were calculated from their UV-Vis/DRS spectra based on the method proposed by Kumar et al. [36] using the following equation:

$$\alpha h\nu = \left(Ah\nu - E_g\right)^{n/2}, \qquad (1)$$

where $E_g$ is the band gap (eV), $\nu$ is the light frequency, $A$ is the absorption constant, $h$ is Planck's constant, and $\alpha$ is the absorption coefficient. The band gap $E_g$ values of Al-MCM-41@$TiO_2$, Al-MCM-41@0.05Ag/$TiO_2$, Al-MCM-41@0.1Ag/$TiO_2$, and Al-MCM-41@0.15Ag/$TiO_2$ were 3.20, 2.9, 2.83, and 2.81 eV, respectively. These results indicated that the dispersion of silver nanoparticles on $TiO_2$ increases the absorption of light in the visible region and narrows their band gaps. In addition, the Ag nanoparticles acted as electron traps to inhibit recombination [37], which may be beneficial for improving the catalytic activity of the catalysts.

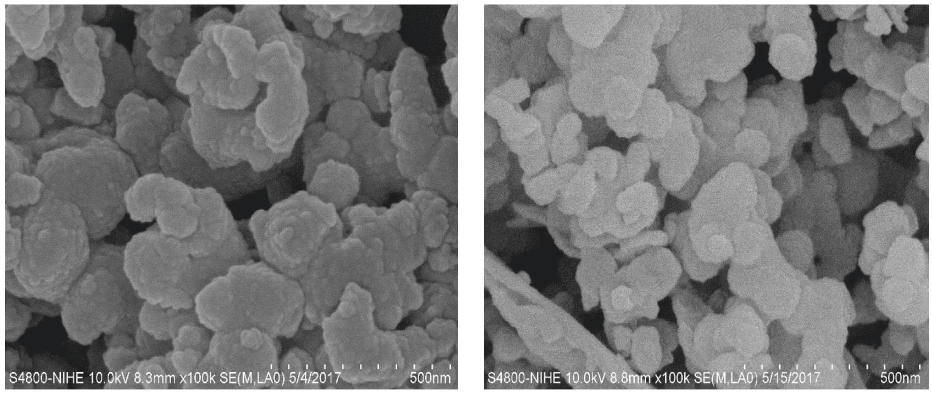


(a) (b)

Figure 2: SEM images of (a) Al-MCM-41 and (b) Al-MCM-41@0.1Ag/$TiO_2$.

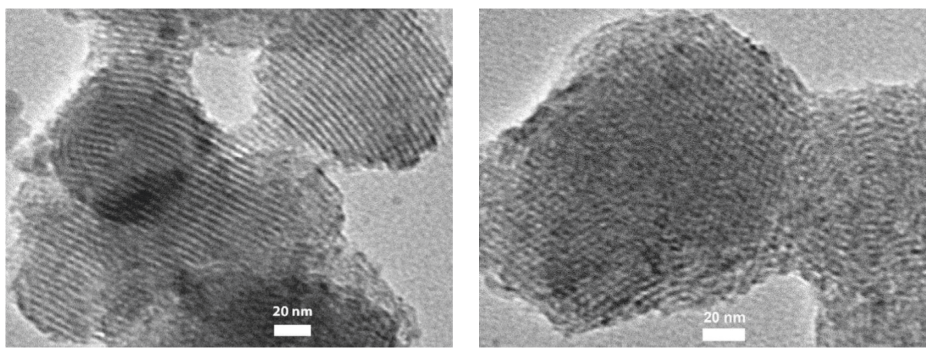


(a) (b)

Figure 3: TEM images of Al-MCM-41@0.1Ag/$TiO_2$.

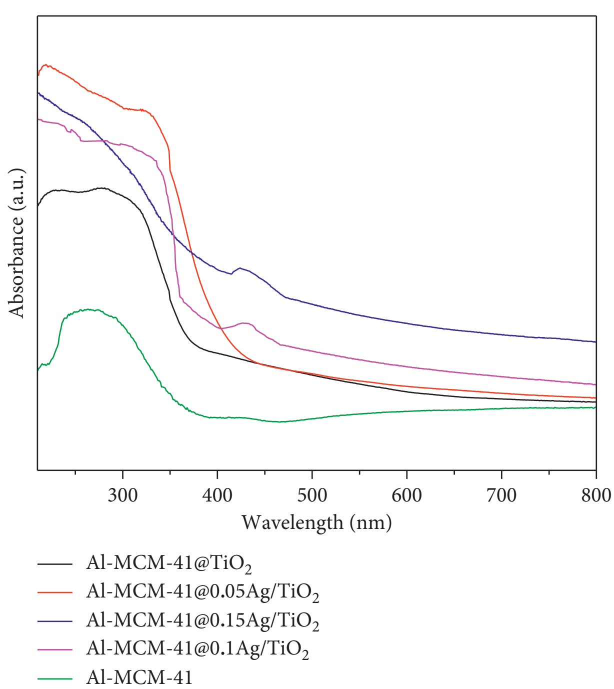


Figure 4: UV-Vis diffuse reflectance spectra of Al-MCM-41@0.15Ag/$TiO_2$, Al-MCM-41@0.1Ag/$TiO_2$, Al-MCM-41@0.05Ag/$TiO_2$, Al-MCM-41@$TiO_2$, and Al-MCM-41.

The EDX of Al-MCM-41@0.1Ag/$TiO_2$ (Figure 5) confirmed the presence of the elements of O, Si, Al, Ti, and Ag with no other impurities observed. The weight percentage of Ag loaded into $TiO_2$ was 6.01% (corresponding to Ag/Ti = 0.095), which is very close to the calculated value of Ag/Ti = 0.1. The EDX analysis of the Al-MCM-41@0.1Ag/$TiO_2$ sample revealed a Si/Al ratio of about 12. This value confirmed that a fairly high amount of aluminum obtained from the Vietnamese bentonite was incorporated into the structure of silica MCM-41.

The $N_2$ adsorption-desorption isotherms of Al-MCM-41 and Al-MCM-41@0.1Ag/$TiO_2$ were typical for type IV, with a hysteresis loop characteristic of mesoporous materials (Figure 6). The calculated specific surface area ($S_{BET}$) of Al-MCM-41 was 633 $m^2 \cdot g^{-1}$ with a pore volume of 0.9 $cm^3 \cdot g^{-1}$ and of Al-MCM-41@0.1Ag/$TiO_2$ was 144 $m^2 \cdot g^{-1}$ with a pore volume of 0.3 $cm^3 \cdot g^{-1}$. The specific surface area and mesoporous volume of Al-MCM-41 loading Ag/$TiO_2$ were lower than those of the pristine Al-MCM-41, which is due to the blocking of some pores by the doping of Ag/$TiO_2$ nanoparticles.

XPS analysis was carried out to analyze the surface composition and chemical states of Al-MCM-41@0.1Ag/$TiO_2$ (Figure 7(a)). The spectrum confirmed the presence of O, Si, Al, Ti, and Ag elements without any other impurities. Figure 7(b) is the high-resolution XPS spectrum

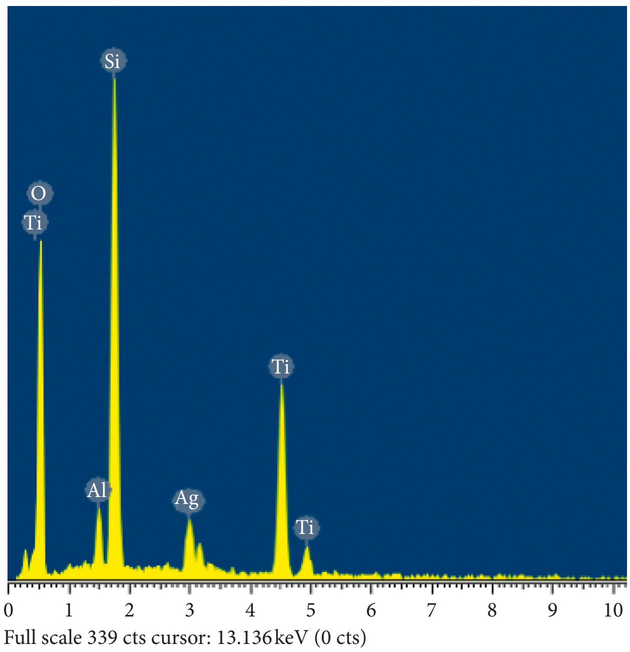


FIGURE 5: EDX spectrum of Al-MCM-41@0.1Ag/$TiO_2$.

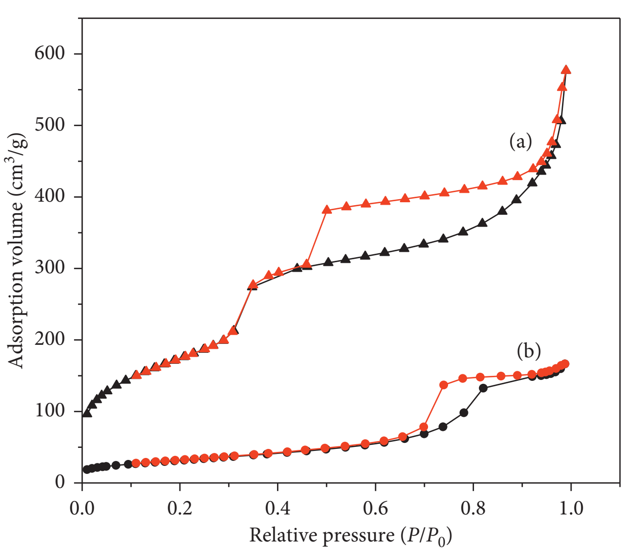


FIGURE 6: $N_2$ adsorption-desorption isotherms of (a) Al-MCM-41 and (b) Al-MCM-41@0.1Ag/$TiO_2$.

of Ag *3d* of Al-MCM-41@0.1Ag/$TiO_2$. Two observed energy bands at 367.51 eV and 373.51 eV correspond to Ag $3d_{5/2}$ and Ag $3d_{3/2}$ of metallic silver. These bands are slightly lower than the bulk Ag metal at 368 eV and 374 eV indicating a strong interaction between Ag and $TiO_2$. The splitting energy between Ag $3d_{5/2}$ and Ag $3d_{3/2}$ is 6 eV, which further confirmed the existence of metallic Ag nanoparticles in the synthesized Al-MCM-41@0.1Ag/$TiO_2$ material [35, 38]. It is also clearly observed that the presence of two different peaks for Ag $3d_{5/2}$ binding energies at 368.1 eV and 367.6 eV were assigned to metallic silver ($Ag^0$) and silver ions in $Ag_2O$ ($Ag^+$), respectively [39]. Thus, partially oxidized metallic Ag nanoparticles were deposited on the $TiO_2$ surface during the synthesis. Figure 7(c) is the high-resolution XPS spectrum of Ti *2p* of Al-MCM-41@0.1Ag/$TiO_2$. Ti *2p* consists of two peaks at 458.48 eV and 464.18 eV (splitting energy = 5.7 eV) which are in accordance with Ti $2p_{3/2}$ and Ti $2p_{1/2}$ of $Ti^{4+}$ in Ag/$TiO_2$ nanostructures, respectively [35, 40].

*3.2. Photocatalytic Activity of Nanocomposite.* The photocatalytic performance of Al-MCM-41@Ag/$TiO_2$ with different Ag loadings was evaluated by the oxidative desulfurization of DBT in the model fuel under the visible light source in 30 minutes at 70°C. The photocatalyst with low Ag loading (0.5wt % Ag/$TiO_2$) exhibited a weak performance (conversion of DBT~48%) due to the low concentration of active catalytic sites, whereas the highest efficiency was obtained for Al-MCM-41@0.1Ag/$TiO_2$ (78% DBT conversion). Due to more silver decorated on the surface of $TiO_2$ for Al-MCM-41@0.15Ag/$TiO_2$ compared with Al-MCM-41@0.1Ag/$TiO_2$, although they have almost the same band gaps, the overlapping of the plasmonic field region makes the photocatalytic activity of Al-MCM-41@0.15Ag/$TiO_2$ mesoporous structure decline (conversion of DBT is 65%). However, overloading of Ag will reduce the amount of available active sites due to the spatial charge repulsion, thereby affecting the photoactivity. Hence, Al-MCM-41@0.1Ag/$TiO_2$ as a photocatalyst has the best photocatalytic activity due to its suitable plasma resonance band, narrow band gap, and available active sites, which is also consistent with the literature [41–43]. Al-MCM-41@0.1Ag/$TiO_2$ photocatalyst was then chosen to carry out the next catalytic tests.

For comparison, the degradation of DBT over Al-MCM-41@$TiO_2$ by the irradiation of UV and visible light was carried out. At 70°C and after 2 hours, the Al-MCM-41@$TiO_2$ photocatalyst degraded only about 40% of DBT under UV light (Figure 8), and almost negligible degradation was observed under visible light (not shown). Compared with Al-MCM-41@$TiO_2$ sample, Al-MCM-41@0.1Ag/$TiO_2$ exhibited remarkably enhanced photocatalytic activities under the same visible light and UV irradiation. The photodegradation efficiencies of DBT increased to almost 100% after 2 h, at 70°C (Figure 8). The improved photocatalytic activity of nanocomposite is due to the strong UV and visible light absorption of Al-MCM-41@0.1Ag/$TiO_2$ material. The Al-MCM-41 support with a large surface area will increase the ability to disperse the catalytic activity center, which will increase the catalytic activity. The surface plasmon resonance of silver nanoparticles was in the visible light region, leading to efficiently absorbing visible light irradiation. In addition, the excellent conductivity of silver nanoparticles may improve electron mobility to enhance the transfer of surface charge to the boundary and prevent the recombination of electrons and holes. Al-MCM-41 acted as an adsorbent in the reaction. By using the sol-gel method, the $TiO_2$ silver-modified silver nanoparticles were homogeneously distributed in ethanol, thereby well dispersed on the pristine material through an intermediate polymer layer of F-127. F-127 played a very important role in $TiO_2$-coated denaturing with Ag because without F-127 $TiO_2$, nanoparticles are difficult to bond with Al-MCM-41 formed. On

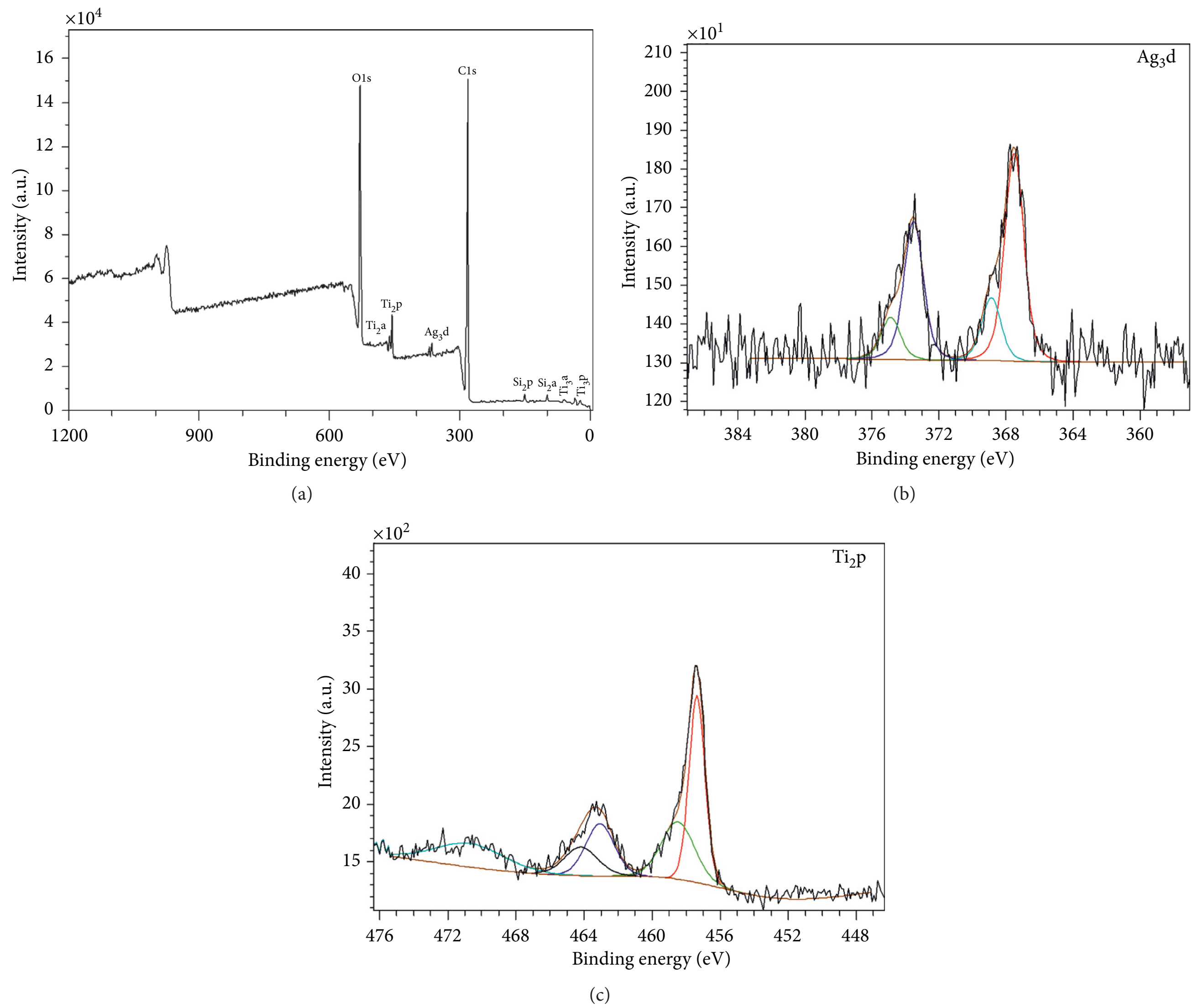


Figure 7: XPS spectra of (a) Al-MCM-41@0.1Ag/$TiO_2$, (b) $Ag_3d$, and (c) $Ti_2p$.

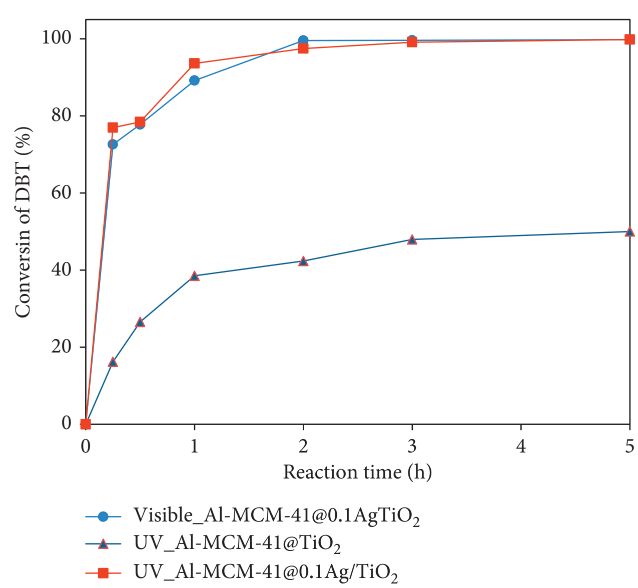


Figure 8: Conversion of DBT over Al-MCM-41@$TiO_2$ and Al-MCM-41@0.1Ag/$TiO_2$ under UV/visible light irradiation. Experimental conditions: $V$ (model fuel) = 20 mL, $m_{\text{Al-MCM-41@0.1Ag/TiO}_2}$ = 0.05 g, $V_{H_2O_2}$ = 0.5 mL, and $T$ = 70°C.

the other hand, Al-MCM-41 covered with F-127 to help disperse the $TiO_2$ nanoparticles onto the surface. The F-127 also protected the hexagonal structure of Al-MCM-41 in the core without being broken down during synthesis. Teng et al. [44] showed that $SiO_2$ not only played a role in the dispersion of $TiO_2$ but also protected the $Fe_3O_4$ core and prevented the core from dissolving into the solution in the formation of the sandwich structure of $Fe_3O_4@SiO_2@TiO_2$.

The effect of temperature on the oxidative desulfurization of DBT during UV and visible irradiations are shown in Figures 9 and 10. It can be seen that as the temperature increased from 30°C to 70°C under both UV and visible light, the conversion of DBT increased and reached 100% at 70°C after 2 hours. The results are in good agreement with literature that increase in the reaction temperature improves the photodegradation efficiency [45].

After 2 h at the reaction temperature slightly above room temperature (30°C), the deep desulfurization could be achieved with 89% and 81% conversions under UV and visible light irradiation, respectively. This was attributed to the formation of conduction band (CB) electrons ($e^-$) and valence band (VB) holes ($h^+$) under irradiation. This indicates that the visible light absorption of $TiO_2$ samples was considerably improved by adding Ag and Al-MCM-41 to $TiO_2$.

Al-MCM-41 has a uniform pore structure and high surface area, which facilitates the high adsorption of DBT. The Ag nanoparticles were photoexcited to enable the generation of electron and $Ag^+$ ($h^+$) due to the surface plasmon resonance effect, and the photoexcited electrons can be further introduced into the conduction band of $TiO_2$ (Equation (2)) [34]. The next possible reaction steps could happen as follows:

$$\mathrm{Ag} + \text{visible light} \longrightarrow \bar{e} + \mathrm{Ag}^+(\mathrm{h}^+) \quad (2)$$

$$\mathrm{TiO_2} + h\nu \longrightarrow \mathrm{h}^+_{\mathrm{VB}} + \bar{e}_{\mathrm{CB}} \quad (3)$$

$$\mathrm{TiO_2}(\bar{e}) + \mathrm{O_2} \longrightarrow \mathrm{O_2^{\bullet-}} \quad (4)$$

$$\mathrm{H_2O_2} + \bar{e} \longrightarrow {}^{\bullet}\mathrm{OH} + \mathrm{HO^-} \quad (5)$$

$$\mathrm{Ag}^+(h^+);\ {}^{\bullet}\mathrm{OH};\ \mathrm{O_2^{\bullet-}};\ \bar{e} + \mathrm{DBT} \longrightarrow \text{degradation products} \quad (6)$$

Species $^{\bullet}OH$ and $O_2^{\bullet-}$ obtained in the presence of the photocatalyst and $H_2O_2$ as the oxidant under irradiation could effectively oxidize DBT to its corresponding sulfone [46]. $Ag^+$ ($h^+$) ions were reactive radical species, which were able to oxidize DBT and reduce to metallic silver. Thus, Ag could be rapidly regenerated, and the Al-MCM-41@0.1Ag/$TiO_2$ composites remained stable.

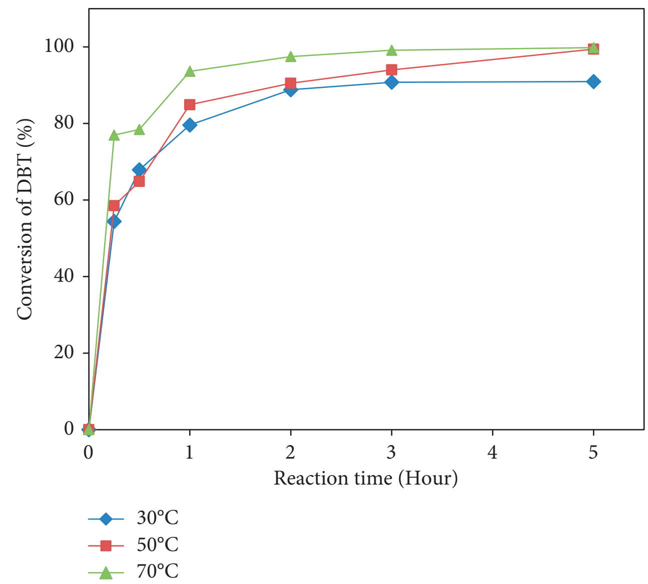


Figure 9: Conversion of DBT under UV at various reaction temperatures. Experimental conditions: $V$ (model fuel) = 20 mL, $m_{\text{Al-MCM-41@0.1Ag/TiO}_2}$ = 0.05 g, and $V_{H_2O_2}$ = 0.5 mL.

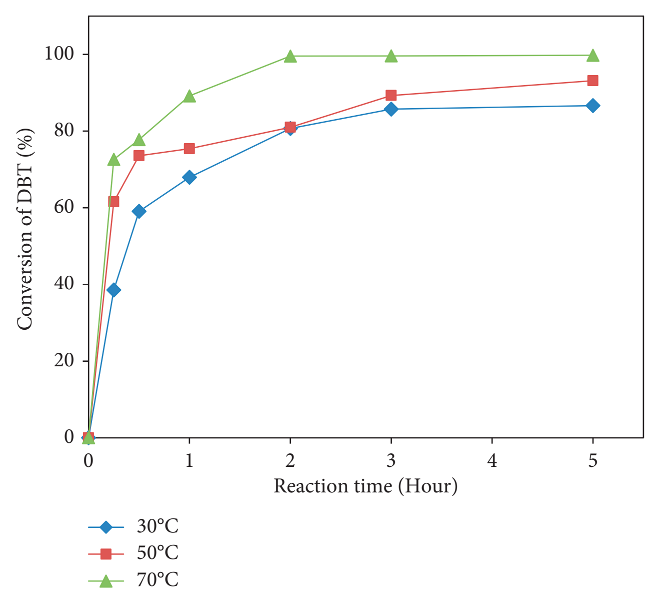


Figure 10: Conversion of DBT under visible irradiation at various reaction temperatures. Experimental conditions: $V$ (model fuel) = 20 mL, $m_{\text{Al-MCM-41@0.1Ag/TiO}_2}$ = 0.05 g, and $V_{H_2O_2}$ = 0.5 mL.

## 4. Conclusions

In summary, the Al-MCM-41@Ag/$TiO_2$ nanocomposites have been successfully synthesized using the Vietnamese bentonite as Si and Al sources and well characterized by various analytical techniques. Al-MCM-41@Ag/$TiO_2$ composites exhibited much higher photocatalytic activities for degrading DBT under visible light irradiation than Al-MCM-41@$TiO_2$, and Al-MCM-41@0.1Ag/$TiO_2$ was found to have the best photocatalytic performance. Incorporating Ag and $TiO_2$ into Al-MCM-41 substrate had positive effects on the photocatalytic activity of the $TiO_2$, under both visible light and UV irradiations. At a relatively mild condition of 30°C, DBT degraded 90% under UV light irradiation and 81% under visible light after 2h. At higher temperature (70°C), the DBT photooxidative desulfurization efficiency of 100% could be achieved after 2 hours under visible light. The Ag nanoparticle dispersed on Al-MCM-41@$TiO_2$

nanocomposites has shown its superiority and the potential as a promising material for the removal of toxic organic pollutants either in the UV or visible light region.

## Data Availability

The data used to support the findings of this study are available from the corresponding author upon request.

## Conflicts of Interest

The authors declare that they have no conflicts of interest.

## Acknowledgments

This work was funded by the Vietnam National Foundation for Science and Technology Development (NAFOSTED) (grant number 105.99-2015.21).

## Supplementary Materials

The results of the HPLC analysis of the conversion of DBT were investigated over time at various reaction temperatures under UV and visible irradiation conditions using Al-MCM41@0.1Ag/$TiO_2$ and Al-MCM-41@$TiO_2$ catalysts. (*Supplementary Materials*)

## References

[1] T. V. Choudhary, S. Parrott, and B. Johnson, "Unraveling heavy oil desulfurization chemistry: targeting clean fuels," *Environmental Science and Technology*, vol. 42, no. 6, pp. 1944–19647, 2008.

[2] C. Song, "An overview of new approaches to deep desulfurization for ultra-clean gasoline, diesel fuel and jet fuel," *Catalysis Today*, vol. 86, no. 1–4, pp. 211–263, 2003.

[3] S. Otsuki, T. Nonaka, N. Takashima, W. Qian, A. Ishihara, and T. Imai, "Oxidative desulfurization of light gas oil and vacuum gas oil by oxidation and solvent extraction," *Energy and Fuels*, vol. 14, no. 6, pp. 1232–1239, 2000.

[4] S. Y. Lee and S. J. Park, "$TiO_2$ photocatalyst for water treatment applications," *Journal of Industrial and Engineering Chemistry*, vol. 19, no. 6, pp. 1761–1769, 2013.

[5] M. A. Kebede, M. E. Varner, N. K. Scharko, R. B. Gerber, and J. D. Raff, "Photooxidation of ammonia on $TiO_2$ as a source of NO and $NO_2$ under atmospheric conditions," *Journal of the American Chemical Society*, vol. 135, no. 23, pp. 8606–8615, 2013.

[6] M. A. Henderson, "A surface science perspective on $TiO_2$ photocatalysis," *Surface Science Report*, vol. 66, no. 6–7, pp. 185–297, 2011.

[7] S. Ardo and G. J. Meyer, "Photodriven heterogeneous charge transfer with transition-metal compounds anchored to $TiO_2$ semiconductor surfaces," *Chemical Society Reviews*, vol. 38, no. 1, pp. 115–164, 2009.

[8] A. A. Ismail and D. W. Bahnemann, "Mesoporous titania photocatalysts: preparation, characterization and reaction mechanisms," *Journal of Material Chemistry*, vol. 21, no. 32, pp. 11686–11707, 2011.

[9] J. Jiang, H. Li, and L. Zhang, "New insight into daylight photocatalysis of AgBr@Ag: synergistic effect between semiconductor photocatalysis and plasmonic photocatalysis," *Chemistry–A European Journal*, vol. 18, no. 20, pp. 6360–6369, 2012.

[10] F. B. Li and X. Z. Li, "The enhancement of photodegradation efficiency using Pt–$TiO_2$ catalyst," *Chemosphere*, vol. 48, no. 10, pp. 1103–1111, 2002.

[11] Y. Borensztein, L. Delannoy, A. Djedidi, R. G. Barrera, and C. Louis, "Monitoring of the plasmon resonance of gold nanoparticles in Au/$TiO_2$ catalyst under oxidative and reducing atmospheres," *Journal of Physical Chemistry C*, vol. 114, no. 19, pp. 9008–9021, 2010.

[12] Y. Yu, W. Wen, X. Y. Qian, J. B. Liu, and J. M. Wu, "UV and visible light photocatalytic activity of Au/$TiO_2$ nanoforests with anatase/rutile phase junctions and controlled Au locations," *Scientific Reports*, vol. 7, article 41253, 2017.

[13] N. Mandzy, E. Grulke, and T. Druffel, "Breakage of $TiO_2$ agglomerates in electrostatically stabilized aqueous dispersions," *Powder Technology*, vol. 160, no. 2, pp. 121–126, 2005.

[14] Q. Zhang, J. B. Joo, Z. Lu et al., "Self-assembly and photocatalysis of mesoporous $TiO_2$ nanocrystal clusters," *Nano Research*, vol. 4, no. 1, pp. 103–114, 2011.

[15] S. Son, S. H. Hwang, C. Kim, J. Y. Yun, and J. Jang, "Designed synthesis of $SiO_2$/$TiO_2$ core/shell structure as light scattering material for highly efficient dye-sensitized solar cells," *ACS Applied Materials and Interfaces*, vol. 5, no. 11, pp. 4815–4820, 2013.

[16] A. Hanprasopwattana, T. Rieker, A. G. Sault, and A. K. Datye, "Morphology of titania coatings on silica gel," *Catalysis Letters*, vol. 45, no. 3–4, pp. 165–175, 1997.

[17] H. Lachheb, O. Ahmed, A. Houas, and J. P. Nogier, "Photocatalytic activity of $TiO_2$–SBA-15 under UV and visible light," *Journal of Photochemistry and Photobiology A: Chemistry*, vol. 226, no. 1, pp. 1–8, 2011.

[18] W. T. Qiao, G. W. Zhou, X. T. Zhang, and T. D. Li, "Preparation and photocatalytic activity of highly ordered mesoporous $TiO_2$–SBA-15," *Material Science and Engineering C*, vol. 29, no. 4, pp. 1498–1502, 2009.

[19] W. J. J. Stevens, K. Lebeau, M. Mertens, T. G. Van, P. Cool, and E. F. Vansant, "Investigation of the morphology of the mesoporous SBA-16 and SBA-15," *Journal of Physical Chemistry B*, vol. 110, no. 18, pp. 9183–9187, 2006.

[20] M. Asiltürk and Ş. Şener, "$TiO_2$-activated carbon photocatalysts: preparation, characterization and photocatalytic activities," *Chemical Engineering Journal*, vol. 180, pp. 354–363, 2012.

[21] A. C. Martins, A. L. Cazetta, O. Pezoti, J. R. B. Souza, T. Zhang, and E. J. Pilau, "Sol-gel synthesis of new $TiO_2$/activated carbon photocatalyst and its application for degradation of tetracycline," *Ceramics International*, vol. 43, no. 5, pp. 4411–4418, 2017.

[22] E. Amereh and S. Afshar, "Photodegradation of acetophenone and toluene in water by nano-$TiO_2$ powder supported on NaX zeolite," *Material Chemitry and Physics*, vol. 120, no. 2–3, pp. 356–360, 2010.

[23] T. Kamegawa, Y. Ishiguro, R. Kido, and H. Yamashita, "Design of composite photocatalyst of $TiO_2$ and Y-zeolite for degradation of 2-propanol in the gas phase under UV and visible light irradiation," *Molecules*, vol. 19, no. 10, pp. 16477–16488, 2014.

[24] S. Abedi and A. Morsali, "Ordered mesoporous metal–organic frameworks incorporated with amorphous $TiO_2$ as photocatalyst for selective aerobic oxidation in sunlight irradiation," *ACS Catalysis*, vol. 4, no. 5, pp. 1398–1403, 2014.

[25] A. Crake, K. C. Christoforidis, A. Kafizas, S. Zafeiratos, and C. Petit, "$CO_2$ capture and photocatalytic reduction using

bifunctional $TiO_2$/MOF nanocomposites under UV–vis irradiation," *Applied Catalysis B: Environmental*, vol. 210, pp. 131–140, 2017.

[26] S. M. V. Phanikrishna, K. V. Durga, and M. Subrahmanyam, "Photocatalytic degradation of isoproturon herbicide over $TiO_2$/Al-MCM-41 composite systems using solar light," *Chemosphere*, vol. 72, no. 4, pp. 644–651, 2008.

[27] K. C. Park, D. J. Yim, and S. K. Ihm, "Characteristics of Al-MCM-41 supported Pt catalysts: effect of Al distribution in Al-MCM-41 on its catalytic activity in naphthalene hydrogenation," *Catalysis Today*, vol. 74, no. 3–4, pp. 281–290, 2002.

[28] Z. Diao, L. Wang, X. Zhang, and G. Liu, "Catalytic cracking of supercritical n-dodecane over meso-HZSM-5@Al-MCM-41 zeolites," *Chemical Engineering Science*, vol. 135, pp. 452–460, 2015.

[29] S. Rodrigues, S. Uma, I. N. Martyanov, and K. J. Klabunde, "AgBr/Al-MCM-41 visible-light photocatalyst for gas-phase decomposition of $CH_3CHO$," *Journal of Catalysis*, vol. 233, no. 2, pp. 405–410, 2005.

[30] Y. Ling, M. Long, P. Hu, Y. Chen, and J. Huang, "Magnetically separable core–shell structural $\gamma$-$Fe_2O_3$@Cu/Al-MCM-41 nanocomposite and its performance in heterogeneous Fenton catalysis," *Journal of Hazardous Materials*, vol. 264, pp. 195–202, 2014.

[31] T. Ali-dahmane, M. Adjdir, R. Hamacha, F. Villieras, A. Bengueddach, and P. G. Weidler, "The synthesis of MCM-41 nanomaterial from Algerian Bentonite: the effect of the mineral phase contents of clay on the structure properties of MCM-41," *Comptes Rendus Chimie*, vol. 17, no. 1, pp. 1–6, 2014.

[32] H. Yang, Y. Deng, C. Du, and S. Jin, "Novel synthesis of ordered mesoporous materials Al-MCM-41 from bentonite," *Applied Clay Science*, vol. 47, no. 3–4, pp. 351–355, 2010.

[33] L. Liang, Y. Meng, L. Shi, J. Ma, and J. Sun, "Enhanced photocatalytic performance of novel visible light-driven Ag–$TiO_2$/SBA-15 photocatalyst," *Superlattices and Microstructures*, vol. 73, pp. 60–70, 2014.

[34] Q. Xiang, J. Yu, B. Cheng, and H. C. Ong, "Microwave-hydrothermal preparation and visible-light photoactivity of plasmonic photocatalyst Ag-$TiO_2$ nanocomposite hollow spheres," *Chemistry–An Asian Journal*, vol. 5, pp. 1466–1474, 2010.

[35] Y. Zhang, T. Wang, M. Zhou, Y. Wang, and Z. Zhang, "Hydrothermal preparation of Ag-$TiO_2$ nanostructures with exposed {001}/{101} facets for enhancing visible light photocatalytic activity," *Ceramics International*, vol. 43, no. 3, pp. 3118–3126, 2017.

[36] V. Kumar, S. Kr. Sharma, T. P. Sharma, and V. Singh, "Band gap determination in thick films from reflectance measurements," *Optical Materials*, vol. 12, no. 1, pp. 115–119, 1999.

[37] S. Krejčíková, L. Matějová, K. Kočí, L. Obalová, Z. Matěj, and L. Čapek, "Preparation and characterization of Ag-doped crystalline titania for photocatalysis applications," *Applied Catalysis B: Environmental*, vol. 111-112, pp. 119–125, 2012.

[38] L. Zhang, D. Shi, B. Liu, G. Zhang, Q. Wang, and J. A. Zhang, "A facile hydrothermal etching process to in situ synthesize highly efficient $TiO_2$/Ag nanocube photocatalysts with high-energy facets exposed for enhanced photocatalytic performance," *CrystEngComm*, vol. 18, no. 34, pp. 6444–6452, 2016.

[39] P. Prieto, V. Nistor, K. Nouneh, M. Oyama, M. Abd-Lefdil, and R. Díaz, "XPS study of silver, nickel and bimetallic silver–nickel nanoparticles prepared by seed-mediated growth," *Applied Surface Science*, vol. 258, no. 22, pp. 8807–8813, 2012.

[40] L. Xu, E. M. P. Steinmiller, and S. E. Skrabalak, "Achieving synergy with a potential photocatalytic Z-scheme: synthesis and evaluation of nitrogen-doped $TiO_2$/$SnO_2$ composites," *Journal of Physical Chemistry C*, vol. 116, no. 1, pp. 871–877, 2012.

[41] K. H. Leong, B. L. Gan, S. Ibrahim, and P. Saravanan, "Synthesis of surface plasmon resonance (SPR) triggered Ag/$TiO_2$ photocatalyst for degradation of endocrine disturbing compounds," *Applied Surface Science*, vol. 319, pp. 128–135, 2014.

[42] W. Zhao, L. Feng, R. Yang, J. Zheng, and X. Li, "Synthesis, characterization, and photocatalytic properties of Ag modified hollow $SiO_2$/$TiO_2$ hybrid microspheres," *Applied Catalysis B: Environmental*, vol. 103, no. 1-2, pp. 181–189, 2011.

[43] D. Lu, S. Ouyang, H. Xu, D. Li, X. Zhang, and Y. Li, "Designing Au surface-modified nanoporous-single-crystalline $SrTiO_3$ to optimize diffusion of surface plasmon resonance-induce photoelectron toward enhanced visible-light photoactivity," *ACS Applied Material and Interfaces*, vol. 8, no. 14, pp. 9506–9513, 2016.

[44] Z. Teng, X. Su, G. Chen, C. Tian, H. Li, and L. Ai, "Superparamagnetic high-magnetization composite microspheres with $Fe_3O_4$@$SiO_2$ core and highly crystallized mesoporous $TiO_2$ shell," *Colloid and Surface A: Physicochemical Engineering Aspects*, vol. 402, pp. 60–65, 2012.

[45] N. A. M. Barakat, M. A. Kanjwal, I. S. Chronakis, and H. Y. Kim, "Influence of temperature on the photodegradation process using Ag-doped $TiO_2$ nanostructures: negative impact with the nanofibers," *Journal of Molecular Catalysis A: Chemical*, vol. 366, pp. 333–340, 2013.

[46] H. Lu, J. Gao, Z. Jiang, Y. Yang, B. Song, and C. Li, "Oxidative desulfurization of dibenzothiophene with molecular oxygen using emulsion catalysis," *Chemical Communication*, vol. 2, pp. 150–152, 2007.